Stochastic Environmental Research and Risk Assessment 15 (2001) 372–383 © Springer-Verlag 2001

A fractal-multifractal approach to groundwater contamination. 2. Predicting conservative tracers at the Borden site

C. E. Puente, O. Robayo, B. Sivakumar

Abstract. In a companion paper (Puente et al., this issue), the capability of a deterministic fractal-multifractal (FM) approach to faithfully and compactly describe the geometry of chloride and bromide tracers gathered at the Borden site was illustrated. As trends in surrogate parameter space were found for successive plume contours (i.e. linear growth in coordinates by which fractal interpolating functions pass, nearly constant rotations and fairly high scalings), this article reports usage of a variety of prediction schemes, based on linear regressions and the aforementioned trends, in order to study the evolving plumes. It is shown that the FM representation leads to plausible non-Gaussian plume evolutions and yields predictions that closely approximate records for a period of time that extends even beyond one year. It is illustrated that such predicted geometries are also consistent with predictions made via stochastic theories (i.e. Dagan, 1984).

1 Introduction

The first article in this series (Puente et al., this issue) investigated the possible usage of a fractal-based geometric framework for modeling the dynamics of groundwater contamination, interpreting each snap-shot of a plume as a projection off a fractal interpolation function. The application of this approach to the conservative tracers (chloride and bromide) at the Borden site indicate that the fractal-multifractal (FM) method does provide a faithful and compact representation of the evolving plume, as illustrated for ten contour plots as gathered on days 1, 9, 29, 43, 63, 259, 332, 381, 462, and 647 after injection. Having obtained such encouraging results, the present study attempts to use the fractal-geometric framework to predict the movement of the tracers at the site.

As seen in Fig. 4 in Puente et al. (this issue), also reproduced here as Fig. 1, surrogate parameters for successive chloride plume contours; as defined for the two maps yielding the fractal functions:

C. E. Puente (✉), O. Robayo, B. Sivakumar
Department of Land, Air, and Water Resources,
University of California, Davis, CA 95616, USA
Fax: 530-752-5262
e-mail: cepuente@ucdavis.edu

The research leading to this article was supported by Kearney Foundation, as part of the Grant No. 94-19, by the United States Department of Agriculture, as part of the Grant No. 9200544, and by National Science Foundation as part of grant EAR9706623. Valuable comments by anonymous reviewers are acknowledged.

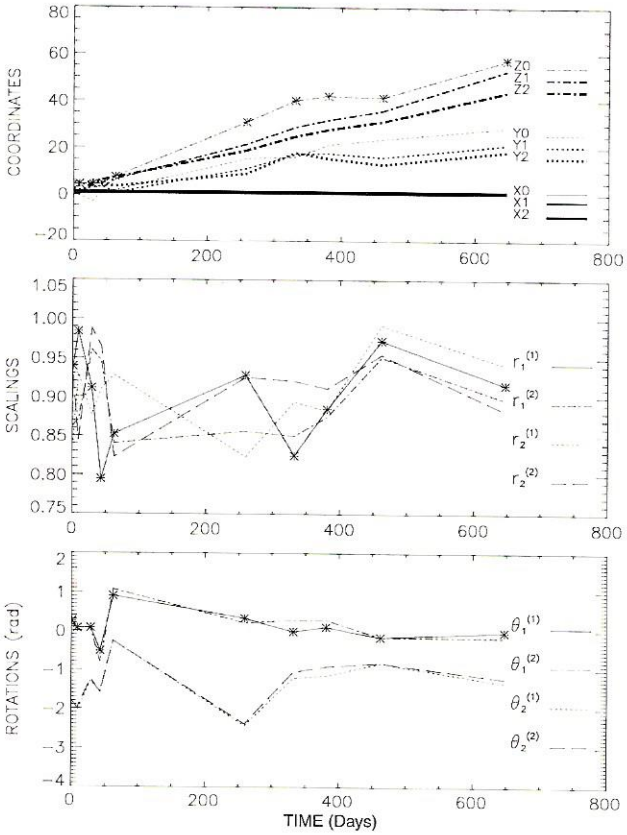

Fig. 1. Evolution of FM surrogate parameters for chloride at the Borden site

$$w_n \begin{pmatrix} x \\ y \\ z \end{pmatrix} = \begin{pmatrix} a_n & 0 & 0 \\ c_n & d_n & h_n \\ k_n & l_n & m_n \end{pmatrix} \begin{pmatrix} x \\ y \\ z \end{pmatrix} + \begin{pmatrix} e_n \\ f_n \\ g_n \end{pmatrix}, \quad n = 1, \ldots, 2 \tag{1}$$

such that

$$w_n \begin{pmatrix} x_0 \\ y_0 \\ z_0 \end{pmatrix} = \begin{pmatrix} x_{n-1} \\ y_{n-1} \\ z_{n-1} \end{pmatrix}, \quad w_n \begin{pmatrix} x_2 \\ y_2 \\ z_2 \end{pmatrix} = \begin{pmatrix} x_n \\ y_n \\ z_n \end{pmatrix}, \tag{2}$$

with the sub-matrix

$$\mathbf{A}_n = \begin{pmatrix} d_n & h_n \\ l_n & m_n \end{pmatrix} \underline{\underline{\text{def}}} \begin{pmatrix} r_n^{(1)} \cos\theta_n^{(1)} & -r_n^{(2)} \sin\theta_n^{(2)} \\ r_n^{(1)} \sin\theta_n^{(1)} & r_n^{(2)} \cos\theta_n^{(2)} \end{pmatrix}, \tag{3}$$

and with the other coefficients, i.e. a_n, c_n, e_n, f_n, g_n, and k_n found in terms of coordinates and $\mathbf{A}_n$ (Puente et al., this issue); exhibited relevant trends that allowed following the plume evolution, as follows. First, there are the coordinates of fractal functions yielding the desired projections, i.e. (x_n, y_n, z_n), $n = 0, 1, 2$, that exhibit a linear growth in the y–z plane [Y–X in Freyberg (1986)].Then, there are

the scalings $r_n^{(i)}$, which have relatively high values for all times (greater than 0.8), and the rotations $\theta_n^{(i)}$, which evolve by couples and appear to stabilize once the plume's track settles down, i.e. after day 332.

The presence of these trends suggests that it may be possible to predict the evolution of the plume via the geometric approach, for times that extend beyond the last observation at day 647 after injection. This study investigates alternative ways in which this goal may be accomplished and compares the results with those reported at the site using stochastic pollution theories.

2 Prediction scenarios

The presence of trends in scalings and rotations for the chloride plume (Fig. 1) (also found for the similarly evolving bromide plume) naturally suggests the possibility of obtaining similar trends when the parameter submatrix A_n, defined above, is studied in Cartesian coordinates. In this light, Fig. 2 shows the behavior of such parameters for the chloride plume, i.e. d_n, h_n, l_n, m_n. Observe that in consonance with Fig. 1, such parameters show noticeable oscillations during the initial stages of the plume(s) and also exhibit varying degrees of "constancy" for the last four dates, i.e. those sampled from 332 days on, yielding additional hope that trends may perhaps be extrapolated in order to study the plumes beyond the last observation date.

As "linear" trends may indeed be visually discerned in Figs. 1 and 2 and as the fractal-geometric methodology has the inherent property of being continuous with respect to all its parameters, i.e. a "small" change in parameters yields a "small" change in the resulting projections (contours), this study investigates the usage of alternative prediction scenarios which are defined based on constancy of parameters or on linear regressions. Explicitly, the following six plausible scenarios, as suggested by Figs. 1 and 2, are considered:

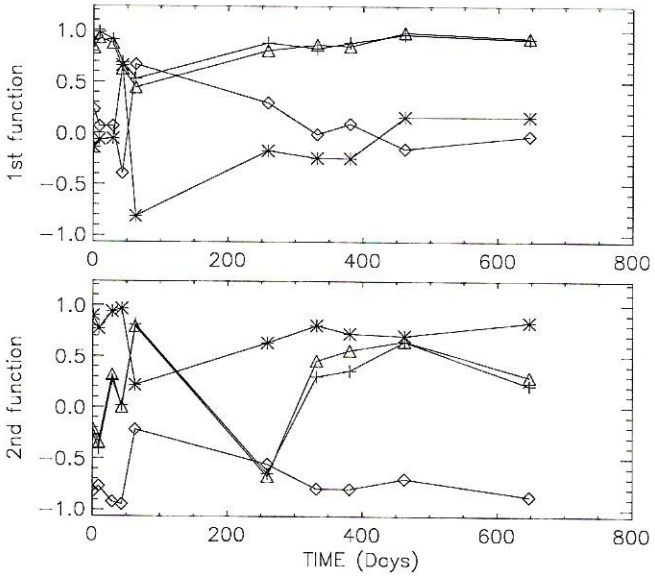

Fig. 2. Evolution of FM Cartesian parameters for chloride at the Borden site $d_n(+), h_n(*), l_n;(\Diamond), m_n(\triangle)$

(a) Case 1: Extrapolation of coordinates (y, z), scalings $(r_n^{(i)})$ and rotations $(\theta_n^{(i)})$ (see Fig. 1) via a line passing by the last two dates, i.e. days 462 and 647 after injection.
(b) Case 2: Same as Case 1, but using best regression lines that interpolate the surrogate parameters for all the ten available dates.
(c) Case 3: Extrapolation of coordinates via a line passing by the last two dates, and usage of constant Cartesian parameter values given by the last date, i.e. day 647 after injection (see Fig. 2).
(d) Case 4: Same as Case 1, except that nearby rotations have been averaged so that sub- matrix A_n is given by only one rotation per mapping rather than two (see Fig. 1).
(e) Case 5: Same as Case 4, except usage of constant scalings given by the last date.
(f) Case 6: Extrapolation of coordinates via the best line passing by the last four dates, extrapolation of rotations via a line passing by the last two dates, and constant scalings given by averages of the last two dates.

Notice that while these scenarios represent a natural variety of forecasting schemes, they also allow further exploration of the projections that may be obtained via the fractal-geometric approach.

An extended analysis of the alternative scenarios, both in a verification and prediction mode, is given next for the chloride plume.

3
Verification Issues

Since most of the prediction scenarios defined above are based on the observations gathered during the last two dates, it is worth studying the kinds of patterns the fractal-multifractal methodology produces with these scenarios at such days. In this regard, Figs. 3 and 4 show the observed vertically averaged concentrations (upper left) and the implied contours as found from five prediction scenarios for days 462 (Cases 1–5) and 647 (Cases 2–6) after injection, respectively.

As can be readily seen in Fig. 3, while all the scenarios correctly preserve the record's center of mass, only Cases 1 and 4 (Fig. 3b and e) yield patterns that may be considered "close" to the observations on day 462 (Fig. 3a). Notice that while Case 1, by definition, corresponds to the best fit found while solving the inverse problem, i.e. with parameters given in Fig. 1 at such a date, Case 4, employing only a single rotation per affine map rather than two, yields a comparable fit. This suggests that having a fractal-multifractal representation with less surrogate parameters has no detrimental effect for such a day. As for all the other scenarios, which are based on regressions passing by all observation dates (Case 2, Fig. 3c) or on Cartesian parameters or scalings defined from day 647 (Case 3, Fig. 3d) and (Case 5, Fig. 3f), respectively), it is seen that the plume's spread is underestimated. This is expected as such shapes reflect the elongation of the plume at day 647, as seen in Fig. 4a.

As seen in Fig. 4, all prediction scenarios, being defined via surrogate values based on day 647, yield patterns that are similar to the actual records for that day. As found earlier, Case 1 (not shown as it is the best FM fit similar to the observations) and Case 4 (Fig. 4d) yield very similar patterns, confirming that there is no significant effect in using two rotations rather than four. In regards to the other scenarios, one may readily notice that they produce properly oriented contours that have varying degrees of transversal dispersion, with Case 2 (based on all ten dates) (Fig. 4b) giving minimal spread and Case 6 (based on last four dates)

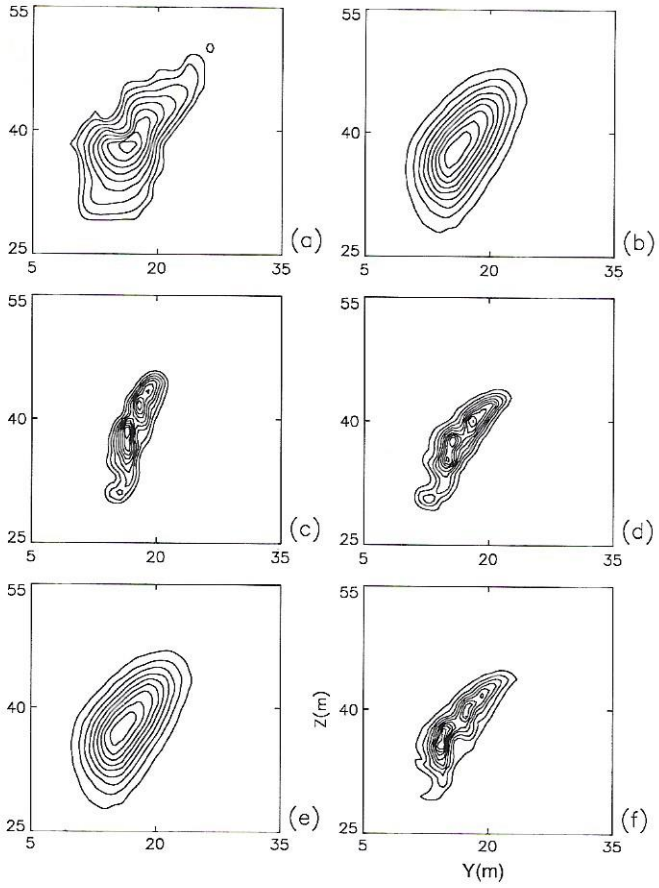

Fig. 3a–f. Observed and fitted chloride profiles for day 462. **a** Observed records, **b** Case 1, **c** Case 2, **d** Case 3, **e** Case 4, **f** Case 5. See text for definition of prediction scenarios

(Fig. 4f) yielding maximal width. Notice that, as expected, Cases 3–5 (all defined based on the last two dates) (Figs. 4c–e) give rather similar patterns for this date.

As all patterns in Figs. 3 and 4 are produced via prediction scenarios whose y and z coordinates are either identical (Cases 1, 3, 4 and 5) or close (Cases 2 and 6), these results suggest that such surrogate parameters prescribe the plume's center of mass. This observation also hints that the precise shape of a fractal-multifractal pattern is given by the interplay of all other surrogate parameters.

4
Prediction results

Predicted chloride patterns at the Borden site for days 750, 900 and 1050 after injection, as produced by the fractal-multifractal method employing the six extrapolation scenarios defined before, are shown in Figs. 5–7.

As seen in Fig. 5, and as expected due to the continuity of the fractal-geometric approach, predicted patterns for day 750 give similar shapes to those found for day 647 (Fig. 4). While all "plumes" from different scenarios continue to spread and move, the trends found in Fig. 4 regarding the different cases remain. Notice how Cases 1, 3, 4, and 5 (Fig. 5a, c, d, e), all relying on the last two dates for their inferences, yield similar profiles inheriting the "narrow s" geometry present in the

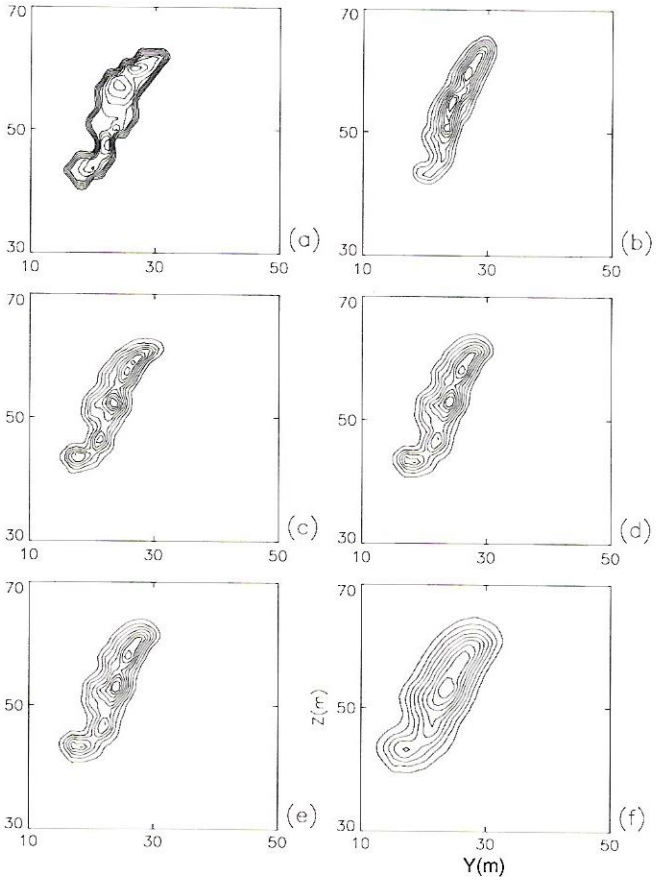

Fig. 4a–f. Observed and fitted chloride profiles for day 647. **a** Observed records, **b** Case 2, **c** Case 3, **d** Case 4, **e** Case 5, **f** Case 6. See text for definition of prediction scenarios

last observation day, and exhibit a host of internal mounds, especially Cases 1 and 4, which only differ in the number of rotations they employ. Observe that, as before, while Case 2 (relying on all available information) yields the narrowest and most elongated plume (Fig. 5b), Case 6 still gives the widest plume (Fig. 5f).

As observed in Figs. 6 and 7, the alternative extrapolation scenarios, while maintaining some of the previous trends, yield noticeably different chloride "plumes" for days 900 and 1050 after injection. The main trends inferred from these patterns are as follows:

(a) plumes obtained using Cases 1 and 4, previously identified as "nearby" scenarios, yield increasingly broken patterns that, although are not as close as they were for earlier dates, share a common texture (Figs. 6a, d and 7a, d).
(b) patterns found via Case 2 continue being narrow and elongated (Figs. 6b and 7b), whereas those produced by Case 6 are increasingly wider (Figs. 6f and 7f). Notice that, consistent with Figs. 4 and 5, the slender plume is more vertically oriented than the wider one.
(c) the plume obtained using Case 3, based on an extrapolation of FM Cartesian parameters for day 647 as seen in Fig. 2, grows and moves with time but maintains its overall "s" shape and orientation (Figs. 6c and 7c).

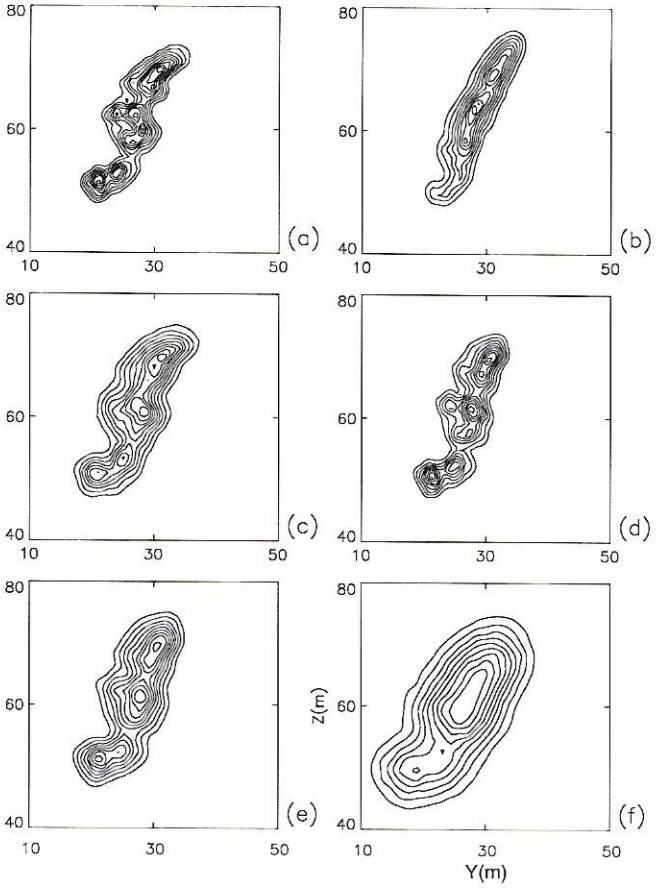

Fig. 5a–f. Predicted chloride profiles for day 750. **a** Case 1, **b** Case 2, **c** Case 3, **d** Case 4, **e** Case 5, **f** Case 6. See text for definition of prediction scenarios

(d) profiles given by Case 5, having fixed scalings corresponding to the last observation date and a fixed rotation averaging those on an affine mapping, grow and progressively orient vertically (Figs. 6e and 7e).

These results, especially those of Case 3 that have all FM Cartesian parameters fixed, confirm that the plume's shape is determined by the interplay of rotations and scalings and show that the coordinates by which a fractal interpolating function passes do dictate the overall location and size of an FM plume. They also illustrate that the fractal-geometric approach may be used to simulate a host of "plausible" patterns that even include some which are made of separate pieces.

In regards to the broken patterns, as given by Cases 1 and 4, it is worth to notice that they happen due to the decreasing trends in FM scalings as implied by the last two dates on Fig. 1. For once such lines are extrapolated, they yield scaling values (from 0.78 to 0.88 for day 900, and from 0.70 to 0.84 for day 1050) which define fractal interpolating functions that progressively fill up less space in three dimensions (Puente and Klebanoff, 1994) that give increasingly disconnected shapes. Notice that although one may be tempted to dismiss these cases as unrealistic, one may also imagine circumstances, with proper medium heterogeneities, in which they may hold.

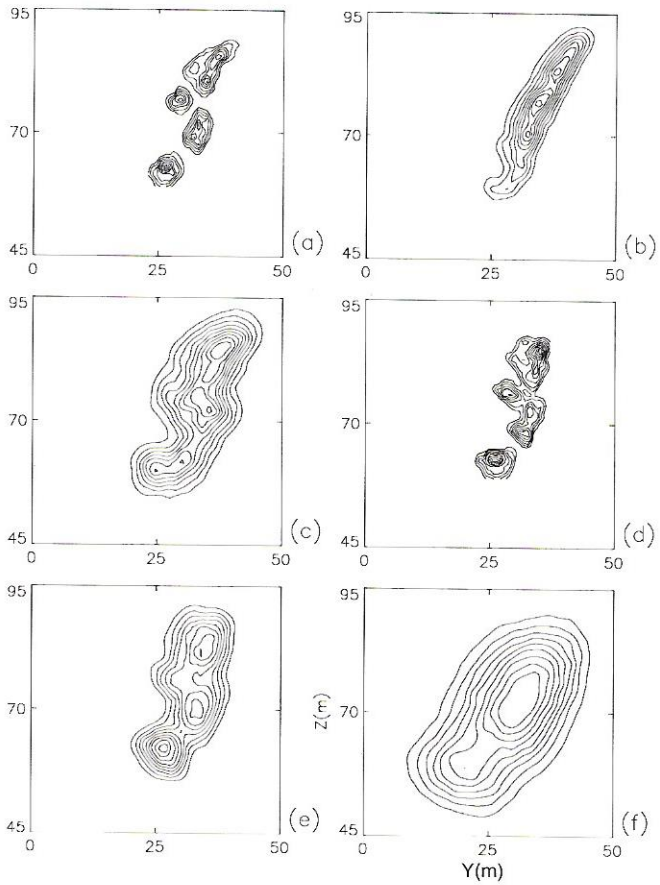

Fig. 6a–f. Predicted chloride profiles for day 900. **a** Case 1, **b** Case 2, **c** Case 3, **d** Case 4, **e** Case 5, **f** Case 6. See text for definition of prediction scenarios

As clear trends regarding the plume's center of mass and dispersion tensor were identified with the records (Freyberg, 1986), it is relevant to study how the alternative evolving plumes behave with respect to these important characteristics. In this light, Fig. 8 presents the patterns' center of mass for all prediction scenarios, and Fig. 9 shows their corresponding covariance tensor.

As can be seen in Fig. 8, which includes real and fitted plumes for all dates, together with patterns from all scenarios for the last two observation dates and predicted profiles every 50 days starting at day 700 and lasting until day 1050 after injection, all prediction scenarios provide patterns that evolve around the 25-degree line (measured clockwise from the vertical), as found with the original records, as follows:

(a) Case 2, ($\triangle$), based on regressions passing by all data points, yields the closest agreement with the 25-degree line, and Case 3, (X), defined by fixed FM Cartesian parameters gives the second best fit with such a line.
(b) Cases 1, 4, and 5, (+, ∇, o), all relying on the last two dates to define the extrapolated coordinates, yield centers of mass close to one another that are steeper than the 25-degree line.

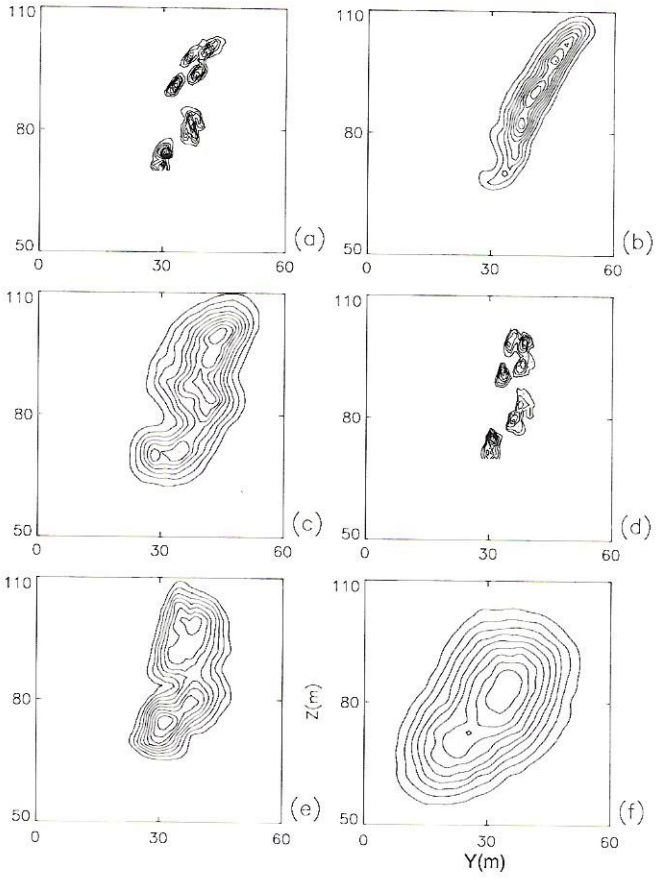

Fig. 7a–f. Predicted chloride profiles for day 1050. **a** Case 1, **b** Case 2, **c** Case 3, **d** Case 4, **e** Case 5, **f** Case 6. See text for definition of prediction scenarios

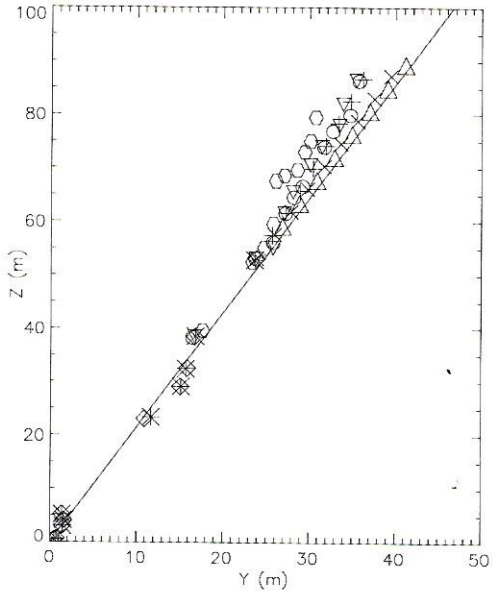

Fig. 8. Evolution of center of mass for chloride at the Borden site. Observed (∗), FM fitted (◊), Case 1 (+), Case 2 (△), Case 3 (X), Case 4 (▽), Case 5 (o), and Case 6 (hexagon). The solid line is at −25° for the Z axis

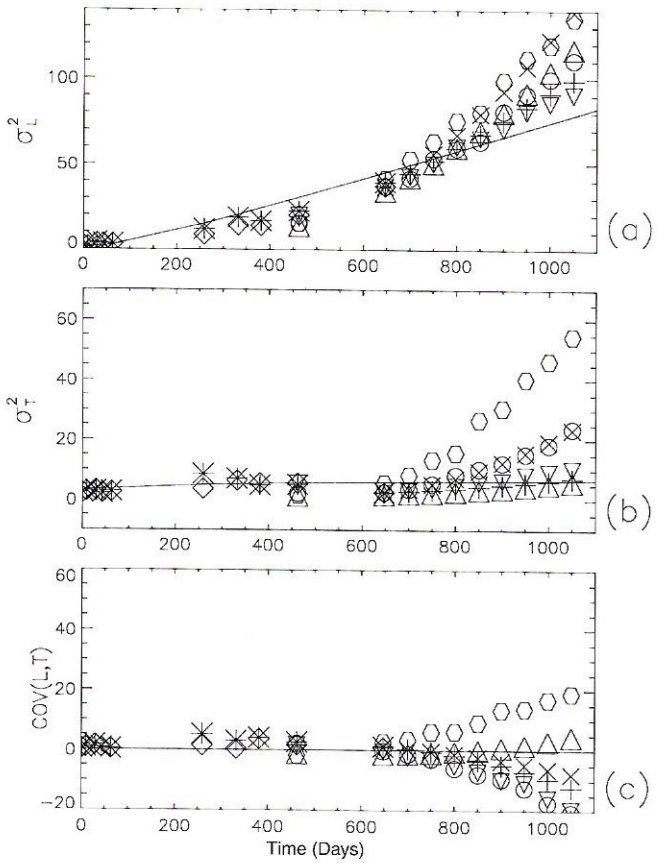

Fig. 9. Evolution of dispersion tensor for chloride at the Borden site. Observed (∗), FM fitted (◊), Case 1 (+), Case 2 (△), Case 3 (X), Case 4 (▽), Case 5 (o), and Case 6 (hexagon). The solid line corresponds to Dagan's model

(c) Case 6, (hexagon), using the last four observation dates, results in the least linear pathway for the center of mass and is the one that deviates most from the 25-degree line.

As can be observed in Fig. 9, more substantial differences among the scenarios can be drawn when considering the longitudinal and transverse dispersions (parallel and perpendicular to the aforementioned 25-degree line), and their cross correlation. As seen, for observed and predicted plumes (every 50 days as in Fig. 8), the following trends may be elucidated:

(a) In regards to the longitudinal variance, all prediction scenarios result in growth, which basically contains two distinct trends. Up until day 800, all scenarios give longitudinal spreads that are close to one another and also close to the variance given by Dagan's model (shown as a solid line), except for Case 6, (hexagon), that gives a larger plume. After day 800, variances grow above Dagan's line in an approximately linear fashion, and in the following order: Case 4, (▽), Case 1, (+), Case 5, (o), Case 2, (△), and Case 3, (X).
(b) With respect to the transverse variance, the prediction scenarios can be divided into three groups. First, Cases 1, (+), 2, (△), and 4, (▽), yield transverse

dispersions which are close to one another and also close to Dagan's predictions, for any day. Second, Cases 3, (X), and 5, (o), give variances that are close to one another, close to Dagan's variance up to day 850 after injection, and increase moderately from then on. Third, Case 6, (hexagon), yields a plume significantly wider than the one implied by Dagan's line.

(c) In regards to the cross-covariances, all scenarios provide values close to zero (Dagan's prediction) for times up to 800 days after injection, except for Case 6 that already yields a positive value. After day 800, only Case 2, (△), continues to have a cross-correlation close to Dagan's model. Whereas Cases 1, 3, 4, and 5 have increasingly negative values from day 800 on, Case 6 has them increasingly positive.

These observations, together with those drawn from the evolution of the center of mass, indicate that the fractal-geometric approach may be used to produce plausible non-elliptical patterns that are consistent with the moments predicted using stochastic theories, for a period of time spanning at least 150 days from the last observation date (up to day 800 after injection). They also illustrate that suitable extrapolation of trends in surrogate FM parameter space may indeed be made which lead to sensible approximations of the evolving plume, that maintain the overall geometries for dates that extend to even 400 days after the last observation date, as observed for Cases 2, 3, and 5.

The appeal of the patterns obtained via the fractal-multifractal approach may also be discerned by comparing the bromide plume gathered at the site on day 1038 after injection with those found for the nearby chloride plume on day 1050, as reported in Fig. 7. As such a real profile did not split into pieces (Freyberg, 1986), one may readily discard the broken patterns predicted using Cases 1 and 4. As the dispersion for the bromide plume ($\sigma_L^2 = 83.3, \sigma_T^2 = 18.8$) is vastly exceeded by the patterns of Case 6 ($\sigma_L^2 \approx 135, \sigma_T^2 \approx 54$), this case may be removed as well.

For the remaining cases (2, 3, and 5), the following detailed comparisons may be made:

(a) As inferred from Fig. 8, the center of mass given by such cases differs from the plume's ($\bar{Y} = 38.1, \bar{Z} = 77.8$) by less than 5% in Y and 11% in Z. This means that those cases' center of mass are within 3 m from that of the observed plume.

(b) As implied by Fig. 9a, the longitudinal variances of 115, 136 and 107 as found for Cases 2, 3, and 5, all exceed the observed value $\sigma_L^2 = 83.3$. This translates in percentage errors in standard deviations which are, in order, 17, 29 and 13%.

(c) As deduced from Fig. 9b, the transverse variances of 5, 22, and 22, as found for the three cases, yield values that in Cases 3 and 5 closely approximate the observed value $\sigma_T^2 = 18.8$. In terms of percentage errors in the standard deviation these cases give, in order, 100, 7, and 7%.

(d) As seen from Fig. 9c, the three scenarios give cross covariances (4, −7, −20) which are far away from the observed value of 13.6 m^2.

Even though none of the prediction scenarios is able to fully capture the plume as seen during day 1038 (as reported in Freyberg, 1986), it is worth remarking that Cases 3 and 5 do provide sensible approximations in regards to the plume's overall orientation and their statistical attributes (except cross correlations). At the end, these non-Gaussian predictions turn out to give a slightly worse performance in longitudinal variance than Dagan's model, but clearly outperform the stochastic framework in regards to the observed transverse variance.

As predictions via the fractal-multifractal methodology have a lead time of more than a year (391 days), these results are remarkable. They suggest that one may indeed understand dynamics from geometry in a fashion that does not require stochastic partial differential equations nor the assumption of elliptical plumes.

5
Summary and final remarks

A study of plausible prediction scenarios capitalizing on trends found via a geometric encoding of chloride patterns as observed in the Borden site (Puente et al., this issue) has been presented. It has been shown that the fractal-geometric procedure, by capturing the most important features present in the records, allows finding reasonable predictions of the evolution of a conservative plume, that besides being consistent with stochastic theories (e.g. Dagan, 1984) for a long period of time (150 days in this case), yields non-Gaussian patterns which provide sensible geometries and close forecasts for an extended lead time (391 days here).

These results indicate that there is a possibility of developing an alternative methodology, i.e. a geometric approach, in order to understand the dynamics of pollutants in groundwater. Such an approach may either be used, by itself, when sufficient records (spatial patterns) are available, or in conjunction with stochastic theories, in order to simulate realistic non-elliptical shapes with appropriate moments.

As a fractal-geometric method not only requires discernible trends on surrogate parameter space but also depends on their presence at larger spatial scales, other case studies need to be considered in order to substantiate the procedure and to establish general links between physical parameters (i.e. dispersivity tensor) and the geometric surrogate parameters. In this regard, it is envisioned that relevant linkages between plume qualifiers and surrogate parameters may be elucidated via extensive simulations.

References

Dagan G (1984) Solute transport in heterogeneous porous formations. J. Fluid Mech. 145: 151–177

Freyberg DL (1986) A natural gradient experiment on solute transport in a sand aquifer. 2. Spatial moments and the advection and dispersion of nonreactive tracers. Water Resour. Res. 22(13): 2031–2046

Puente CE (1996) A new approach to hydrologic modeling: derived distributions revisited. J. Hydrol. 187: 65–80

Puente CE, Klebanoff AD (1994) Gaussians everywhere. Fractals 2(1): 65–79

Puente CE, Robayo O, Diaz MC, Sivakumar B (2001) A fractal-multifractal approach to groundwater contamination. 1. Modeling conservative tracers at the Borden site. Stoch. Envir. Res. Risk Asses. 15: 357–371